Neutral polar wind

Larry C. Gardner and Robert W. Schunk
Center for Atmospheric and Space Sciences, Utah State University, Logan, Utah, USA

Received 14 October 2003; revised 13 February 2004; accepted 24 February 2004; published 5 May 2004.

[1] The classical polar wind is an ambipolar outflow of ions from high latitudes along open geomagnetic field lines. The polar wind consists of light thermal ions (H^+, He^+) and energetic light and heavy ions (H^+, He^+, O^+). The characteristics of these ions have been studied quite extensively since the 1960s. In just the last 20 years, however, energetic neutral atoms (ENAs) that are produced in charge exchange reactions between the singly ionized polar wind ions and the surrounding neutral atoms have been used as a means to remotely probe plasma populations. Recent estimates for neutral outflow integrated fluxes from the LENA instrument on the IMAGE spacecraft have shown values of $1-4 \times 10^9$ cm^{-2} s^{-1}, with a considerable diurnal variation. A theoretical model has been used in this study that is similar to the high-latitude hydrodynamic polar wind model developed at Utah State University, but it has been expanded to include the effects of neutral stream particles so that the characteristics of the neutral polar wind can be elucidated. The neutral polar wind model results show a high neutral hydrogen outflow flux on the order of 10^9 cm^{-2} s^{-1}. *INDEX TERMS:* 2427 Ionosphere: Ionosphere/atmosphere interactions (0335); 2475 Ionosphere: Polar cap ionosphere; 2437 Ionosphere: Ionospheric dynamics; 2776 Magnetospheric Physics: Polar cap phenomena; *KEYWORDS:* exosphere, modeling, polar wind

Citation: Gardner, L. C., and R. W. Schunk (2004), Neutral polar wind, *J. Geophys. Res.*, *109*, A05301, doi:10.1029/2003JA010291.

1. Introduction

[2] Ion outflow occurs at high-latitudes along open magnetic field lines. These open field lines are due to the Earth's intrinsic magnetic field in the polar regions connecting to the Interplanetary Magnetic Field (IMF) and being dragged back toward the tail region. This creates an open field line along which ions originating in the ionosphere can escape from the Earth.

[3] In the polar ionosphere, where the geomagnetic field lines are connected to the IMF, diffusive equilibrium does not occur due to plasma continually flowing into interplanetary space. The loss of plasma, however, exceeds that predicted from evaporation at normal ionospheric temperatures, as suggested by *Dessler and Michel* [1966] and *Nishida et al.* [1966]. *Axford* [1968] pointed out that the lighter ions must be dragged away from the earth by the flux of escaping photoelectrons, and suggested the speed of escape should reach 10 km/sec or more. The ions are accelerated by an electric field that is produced by a charge separation resulting from the escaping photoelectrons. A photoelectron flux with energies greater than 2.4 eV would be sufficient to carry away the lighter ions produced in the ionosphere [*Axford*, 1968]. At higher photoelectron energies even heavier ions may be able to escape. The net result is a topside O^+ scale height that is abnormally large in regions where the geomagnetic field is open and photoelectrons can escape, and the mean ion mass in the same regions will be higher for a given altitude. In regions where the field lines have recently reconnected so that the photoelectrons are no longer able to escape, the flow of ions may decrease to levels appropriate for thermal diffusion. *Axford* [1968] points out that the description of how the ionospheric plasma flows away from the Earth along open geomagnetic field lines is closely analogous to the flow of solar plasma away from the sun, and hence he called this phenomenon the "polar wind."

[4] Open field lines continually sweep across the polar caps and into the tail of the magnetosphere where they eventually reconnect in the vicinity of the neutral sheet [*Axford and Hines*, 1961; *Axford*, 1969]. The reconnected field lines then migrate sunward at relatively low geomagnetic latitudes. During the first part of the convection, following just after the disconnection of the field line, plasma escape occurs when the pressure suddenly decreases on the disconnected plasma tube due to its connection with the interplanetary magnetic field. This sudden pressure drop results in the depletion of H^+ and He^+. The plasma tube then continues its convection across the polar cap until it eventually reconnects in the neutral sheet. *Nishida et al.* [1966] suggested that due to the time it takes for ionospheric ionization to replenish, regions of field line convection would be characterized by low electron concentrations. He then defined the plasmapause boundary as the last field line that does not participate in convection.

[5] It is important to understand the polar wind because it serves as a primary source of magnetospheric plasma [*Shelley et al.*, 1982; *Moore et al.*, 1986a, 1986b; *Chappell et al.*, 1987], and provides the principle means by which

0148-0227/04/2003JA010291$09.00

ionospheric plasma gets transported into the magnetosphere. The study of the processes involved in the polar wind are important because they lead to a better understanding of the coupling through mass, momentum, and energy between the various regions associated with the flow.

[6] Because of magnetospheric electric fields, the high-latitude ionosphere (including the polar wind) is in a continual state of horizontal motion. This horizontal motion is significant because the time it takes the polar wind to flow up and out of the topside ionosphere is comparable to the transit time across the polar cap.

[7] At high latitudes there is a substantial outflow of ionospheric plasma. It consists of light thermal ions (H^+, He^+), and light and heavy energized ions (H^+, He^+, O^+, N^+, NO^+, O_2^+, N_2^+). Thermal outflow of ionospheric ions is associated with the classical polar wind, while energized outflow is associated with auroral energization or non-classical polar wind processes. There are several mechanisms that control this ion outflow. The first of which is the sunlit region. Here photoelectrons heat thermal electrons, which leads to an increase in the polar wind outflow rate, and at high altitudes the escaping photoelectrons can increase the acceleration of the polar wind ions. Another mechanism is associated with the cusp auroral zone. Here precipitating magnetospheric electrons can heat thermal electrons in a manner similar to photoelectrons. Energized ions can also be created in the form of beams and conics by field-aligned auroral currents and potential structures. Cusp beams and conics convecting into the polar cap can destabilize the polar wind as they pass through it, transferring energy to thermal ions. Acceleration mechanisms in the polar cap include Joule heating, hot magnetospheric ions and electrons, electromagnetic wave turbulence, and centrifugal acceleration [cf. *Schunk and Nagy*, 2000].

[8] Energetic neutral atoms (ENAs) are produced in charge exchange reactions between singly ionized ions and the surrounding neutral atoms. In the case of the polar wind, the main ion (H^+, O^+) motion is in the direction of the magnetic field and these ions can experience charge exchange reactions with the surrounding neutral atmosphere (H, O). The resulting charge exchanges produce ENAs that propagate away in the general direction of the magnetic field at the point of the charge exchange. The fluxes of these ENAs are currently unknown.

2. Theoretical Model

[9] In order to study the characteristics of ENAs produced in the polar wind, an ion-neutral transport model, using the numerical method of *Boris and Book* [1976], has been developed which solves the time-dependent continuity and momentum equations for 5 species (O^+, H^+, electrons, H stream, O stream) with charge exchange taken into account. This theoretical model is similar to the high-latitude hydrodynamic model of the polar wind used by *Schunk and Sojka* [1989, 1997] and by *Demars and Schunk* [2002], except that the O and H streams have now been included.

[10] The high-latitude hydrodynamic model solves the time-dependent continuity and momentum equations between 500 km and 9,000 km for H^+, O^+, H_s, and O_s (where the subscript s denotes neutral stream particles) along diverging geomagnetic flux tubes assuming that the pressure obeys the ideal gas law. The time-dependent continuity and momentum equations solved are

$$\frac{\partial n_j}{\partial t} + \nabla \cdot \left(n_j \overline{u}_j\right) = P_j - L_j \tag{1}$$

$$\begin{aligned}\frac{\partial \overline{u}_j}{\partial t} + \nabla \cdot \left(\overline{u}_j \overline{u}_j\right) &= \overline{u}_j \left(\nabla \cdot \overline{u}_j\right) \\ &- \frac{\nabla p_j}{n_j m_j} - \nabla \cdot \overline{\overline{\tau}}_j + \frac{e_j \overline{E}}{m_j} + \overline{G} + \sum_k \nu_{jk} \left(\overline{u}_k - \overline{u}_j\right) \Phi_{jk} \\ &+ \sum \frac{P_j}{n_j} \left(\overline{u}_{j'} - \overline{u}_j\right) - \sum \frac{L_j}{n_j} \left(\overline{u}_{j'} - \overline{u}_j\right),\end{aligned} \tag{2}$$

$$p_j n_j^{-\alpha} = const., \tag{3}$$

$$\frac{T_j^{\perp}}{B} = const, \tag{4}$$

where n and $\overline{u}$ are the number density and drift velocity of a specified species, m is the mass, p is the partial pressure, P and L are the production and loss rates, $\overline{G}$ is the gravitational acceleration, $\overline{\overline{\tau}}$ is the stress tensor, $\overline{E}$ is the electric field (zero for neutrals), k_B is the Boltzmann constant, ν is the collision frequency, Φ is a velocity-dependent correction factor, and subscript j can be either ions, electrons, or neutrals. The last two terms in equation (2) are the momentum production and loss [*Eccles and Raitt*, 1992] and are included only for stream particles, since their contribution to the ion momentum is small.

3. Charge Exchange

[11] The charge exchange mechanisms considered for this study include the accidentally resonant charge exchange between hydrogen ions and neutral oxygen, oxygen ions and neutral hydrogen, hydrogen ions and neutral hydrogen, and oxygen ions and neutral oxygen. Figure 1 demonstrates graphically the charge exchange mechanism.

[12] At altitudes below which the H^+ density is less than the O^+ density and O^+ is the dominant species, the H^+ is in chemical equilibrium with O^+. When H^+ and O^+ are in chemical equilibrium, their densities are controlled by the accidentally resonant charge exchange reaction:

$$O^+ + H \underset{k_r}{\overset{k_f}{\Leftrightarrow}} O + H^+, \tag{5}$$

where the forward (k_f) and reverse (k_r) reaction rates are given by [cf. *Raitt et al.*, 1975; *Barakat and Schunk*, 1987]

$$k_f = 2.5 \times 10^{-11} \left[T_n + \frac{T(O^+)}{16} + 1.2 \times 10^{-8} \left(u(O^+) - u_n\right)^2\right]^{1/2}, \tag{6}$$

$$k_r = 2.2 \times 10^{-11} \left[T(H^+) + \frac{T_n}{16} + 1.2 \times 10^{-8} \left(u(H^+) - u_n\right)^2\right]^{1/2}, \tag{7}$$

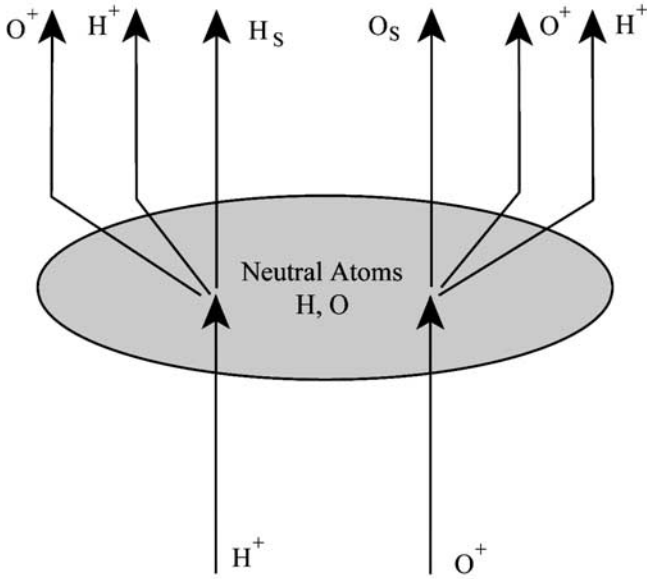

Figure 1. A plot demonstrating the production mechanism for the neutral stream particles. As ions flow through a neutral background, charge exchange occurs between the ion and a neutral, creating a neutral stream particle with the momentum of the parent ion.

where the temperatures are in kelvins, the field-aligned velocities in cm s^{-1}, and the rate coefficients are cm^3 s^{-1}. Production and loss rates for all of the charge exchange combinations mentioned above have been included. Other reactions of interest are listed below:

$$H^+ + H \Rightarrow H + H^+, \tag{8}$$

$$O^+ + O \Rightarrow O + O^+. \tag{9}$$

In reactions (5), (8), and (9) an outflowing ion species is converted into an energetic neutral atom, and the neutral is converted into an ion. Three possible sources for neutral atoms are considered: (1) a thermal neutral background which is taken from the MSIS model, (2) ENAs which then interact with the upflowing ions, and (3) hot geocoronal atoms.

4. Energetic Neutral Atoms

[13] Energetic neutral atoms are produced when an energized ion comes in close proximity to a neutral atom, and an electron is exchanged between the ion and neutral. This produces a new ion and neutral which retain the momentum of the original particles.

[14] ENAs have typically been discussed as coming form the ring current. *Roelof* [1987] discusses ISEE 1 satellite data for stormtime conditions, with the results of the study suggesting peak ion fluxes (H^+ or O^+) in the midnight sector $>10^6$ (cm^2 s sr keV)$^{-1}$, and ENA fluxes from the brighter areas of the satellite image exceeding 10^3 (cm^2 s sr keV)$^{-1}$. *Orsini et al.* [1994] gives a theoretical value for escaping energetic O atoms as 7×10^5 cm^{-2} s^{-1}, and lists several estimates for energetic neutral hydrogen escape fluxes from several sources, ranging from 3×10^2 to 2×10^5 (cm^2 s sr keV)$^{-1}$.

[15] *Orsini et al.* [1994] present a model calculating the expected neutral fluxes from the radiation belts and ring current that would be measured from a satellite in a low altitude orbit (<1500 km). The results show that ENA fluxes on the order of 10^4 (cm^2 s sr kev)$^{-1}$ can be expected for low energies.

[16] *Wilson et al.* [2003] show measurements from the LENA instrument aboard the IMAGE spacecraft for the summer of 2000. Two main sources of ENAs are mentioned, due to two differing patterns in the observed images. The first is highly variable from image to image and has more energetic particles; this pattern could be due to the auroral zone. The second pattern is less variable and is due to lower energy particles; this pattern is possibly from the hot oxygen geocorona. Of note is the integrated flux of O and H neutrals that have a value on the order of $1-4 \times 10^9$ cm^{-2} s^{-1}, and shows a marked diurnal variation of 3×10^9 cm^{-2} s^{-1}.

5. Hot Geocorona

[17] The existence of a non-thermal population of atomic oxygen atoms has been studied for many years. In early investigations, *Hays and Walker* [1966] state that the Doppler profile for the nocturnal green line emission at 5577 Å is markedly non-thermal, with a line width being characteristic of the energy at which the O(^{1}S) atoms are produced. They noted that the green line emission is produced mainly by recombination of atomic oxygen at an altitude of about 100 km, but they also stated that a portion of the emission results from dissociative recombination of O_2^+ ions in the vicinity of the F2 peak. This high altitude emission is characterized by a non-thermal velocity distribution, which is dependent on the production mechanism.

[18] The dissociative recombination of O_2^+ and NO^+ in the *F* region results in atomic oxygen atoms with substantially greater kinetic energy than the ambient atoms, up to several electron volts. *Rohrbaugh and Nisbet* [1973] discussed the characteristics of these energetic oxygen atoms and noted that they have long free paths, thus ascending to altitudes of several thousand kilometers or traveling horizontal distances on the order of the Earth's radius. Their model results show that the energetic oxygen atom density should predominate over the ambient atomic oxygen density above 1000 km under quiet solar conditions, and above 1600 km under disturbed solar conditions. *Torr et al.* [1974], *Torr and Torr* [1979], and *Yee and Hays* [1980] suggested precipitating O^+ as an additional source of atomic oxygen atoms, and *Yee et al.* [1980] observed enhanced oxygen densities at the 550 km level which they ascertain came from dissociative recombination in the daytime and were transported to the nightside along ballistic orbits. The enhanced oxygen densities appeared to be an oxygen geocorona overlying the thermosphere with a number density that was calculated to be about 10^5 to 10^6 cm^{-3} at 550 km. These estimates were taken from twilight airglow observations, and with the assumption that the oxygen atoms were partially thermalized due to collisions, a corresponding temperature of about 4000 K, as observed, would be reasonable.

[19] *Hedin* [1989] showed that a significant population of hot oxygen could be inferred from the differences between existing empirical models and from comparison with in situ

composition measurements at high altitudes. It was found that the summer hot oxygen densities for low to moderate solar activity were $1-3 \times 10^5$ cm^{-3} at 550 km from differences between satellite drag and mass spectrometer based models, and for high solar activity hot oxygen densities of from 5×10^5 to 2×10^6 at 550 km were deduced from a limited number of Dynamics Explorer mass spectrometer measurements. At 1100 km under low solar activity, the cool population of atomic oxygen is a negligible part of the total density, while the hot oxygen densities, based on *Yee et al.* [1980], would be comparable to empirical model total densities.

[20] High-resolution dayglow measurements between the altitudes of 150 km and 960 km were made using the Berkeley EUV airglow rocket [*Cotton et al.*, 1993]. It was found that model estimates for the dayglow underestimated the measurements for look angles greater than the exobase height. This discrepancy could be explained by the existence of an extra source of emission near the exobase. A hot oxygen corona is one possible explanation, while nonlocal thermal equilibrium above the exobase could be another. The two possibilities were modeled with the non-LTE processes showing no effect on the integrated intensities, but the hot oxygen geocorona could explain the measurements. A hot oxygen density of about 10^6 cm^{-3}, with a temperature of 4000 K, is consistent with the data.

[21] Hot oxygen was originally considered to be produced by dissociative recombination of O_2^+ and NO^+, but *Richards et al.* [1994], showed that quenching of metastable species, for winter and high solar activity, can be up to a factor of ten higher than anticipated for their kinetic energy production rates, and therefore could be a significant source of hot oxygen for the exosphere. It was pointed out that a substantial hot oxygen geocorona is important for many reasons, including: maintenance of the nighttime ionosphere, the escape flux of He, and the energetic ion populations in the thermosphere. Current models indicate that the flux from the plasmasphere is not sufficient to maintain the ionospheric densities at the observed levels, so the inclusion of the hot O species may help alleviate this discrepancy. *Shematovich et al.* [1994] used a model based on the Monte Carlo method to solve the nonlinear Boltzmann equation for hot oxygen atoms produced by photodissociation of O_2 and dissociative recombination of O_2^+ and NO^+ atoms at equatorial latitudes for low solar and geomagnetic activity at noon. Their results imply a hot O density at 600 km of about 10^4 cm^{-3}, which is lower than the measured one, but may be corrected by the inclusion of the metastable species hot O production, and a temperature of 4100 K.

[22] *Gérard et al.* [1995] included the metastable species along with the classical species in the model of *Shematovich et al.* [1994]. The inclusion of additional sources of hot O leads to stronger disturbances of the energy distribution function, and thus an increase in the nonthermal fraction of hot O atoms. They therefore calculated a hot O density of 1.2×10^6 cm^{-3} at 550 km for high solar activity, daytime conditions. This is in good agreement with the value of 10^6 cm^{-3} derived from observations.

[23] An adaption of the model for the formation of a hot oxygen geocorona by *Shematovich et al.* [1994] and *Gérard et al.* [1995] was used by *Bisikalo et al.* [1995] for the case of precipitating energetic ions. The model included a full solution of the nonlinear collisional interaction between the thermal ambient gas and superthermal particles, which are produced by O^+ precipitation during magnetic storms. It was found that O^+ precipitation during magnetic storms is a significant source of superthermal oxygen atoms, considerably more than chemical sources alone, yet the temperature of the geocorona remains about 4000 K.

[24] There seems to be agreement that the temperature of the hot O geocorona is about 4000 K and its density is on the order of 1% of the ambient O density at 550 km. The profile for the distribution of hot O with altitude is still, however, in strong disagreement. *Cotton et al.* [1993] suggested a Chapman-like profile, with a peak density near the exobase, a scale height equal to a collisional gas at 4000 K, and a rapid decrease in density below the exobase due to rapid collisional thermalization by the ambient O. *Shematovich et al.* [1994] showed that the hot O was about 1% of the total O at all altitudes above 300 km. Cold O, however, thermally quenches hot O, and higher thermal O densities lead to lower hot O densities. This would then suggest, as in *Cotton et al.* [1993], a Chapman-type layer peaked near the exobase, with a sharp bottomside, and a topside which approaches diffusive equilibrium toward higher altitudes with a scale height appropriate for O at 4000 K.

6. Neutral Stream Simulations

[25] As shown in Figure 1, the upflowing ions (O^+ and H^+) in the polar wind can undergo a charge exchange reaction with the background neutrals (O and H), and this results in neural streams of O and H that predominately flow in the vertical direction (the neutral polar wind). The initial velocity of the neutral particles is equal to the velocity of the O^+ and H^+ parent ions just before the charge exchange process. This velocity can be upward or downward, depending on the background ionospheric and exospheric conditions. Also, the stream dynamics can be different, depending on the geophysical conditions. Therefore the purpose of our study was to determine the characteristics of the neutral streams (direction, flux, drift velocity, and density) for different geophysical conditions. Idealized one-dimensional fluid simulations were conducted for steady state conditions and the resulting O^+, H^+, O and H stream characteristics were calculated.

[26] Two seasonal cases were considered, including summer and winter solstice. For the summer solstice case (day 174) solar maximum conditions were assumed with F10.7 equal to 220. For the winter solstice case (day 355) solar minimum conditions were assumed with F10.7 equal to 70. These cases bracket the range of geophysical conditions that are generally encountered in the upper atmosphere. The MSIS model was used to determine the neutral atmospheric densities, and the neutral atmosphere was assumed to be stationary. In both cases three values of K_p were used; 1, 5, and 8. As noted in section 5, the geocoronal atoms, can be assumed to be either a constant percentage of the neutral density or a Chapman-type layer. In this study, a constant percentage of the neutral density was chosen, since with the assumption of a stationary neutral atmosphere there was virtually no difference between the two layer types. Three sets of chemical reactions were included in the model. The first is the reactions of the outflowing ions with the MSIS

Table 1. Oxygen Boundary Conditions at 500 km for Summer, Solar Maximum, and Winter, Solar Minimum

	O^+		O_s	
	n, cm^{-3}	V, km/s	n, cm^{-3}	V, km/s
Summer				
Solar Maximum	4×10^5	0.0	1×10^5	−0.5
Winter				
Solar Maximum	1×10^4	0.0	1×10^4	−0.5

neutral atmosphere (the thermal neutrals). The second is the reactions of the outflowing ions with the geocoronal atoms, which are at a considerably higher temperature than the thermal neutrals. The third set of reactions is between the outflowing ions and the outflowing neutral polar wind particles, which are created through each of the charge exchange methods. In order to make the model as realistic as possible, the solutions were taken at the north geomagnetic pole, which is where the geomagnetic field lines have the minimum amount of curvature.

[27] The boundary conditions for the model at 500 km were taken from *Schunk and Sojka* [1997] before their magnetic storm was initiated, and the values for the oxygen atoms are listed in Table 1. The boundary conditions at 500 km for the H^+ density were set using equations (5)–(7), and the velocity was set to 0.0 km/s. The boundary conditions at 500 km for the H stream particles vary according to solar activity and time of day. The values used in this study are listed in Table 2. It should be noted that the boundary conditions at 500 km for the H and O streams could not be set arbitrarily. An iterative procedure had to be used until H and O boundary conditions were obtained that were consistent with the ion and neutral flow conditions above 500 km. If the boundary conditions were not set to match the flow conditions above 500 km, a resulting discontinuity would develop at the lower boundary that would result in the termination of the program. For the differing Kp values, and for time of day changes, the flow conditions above 500 km changed, thus resulting in a necessary change in boundary conditions for H stream particles to prevent the discontinuity from forming at the lower boundary; the O steam particles were not as sensitive to Kp and time of day changes. At the upper boundary of the model, free flow conditions were assumed so that particles can escape the topside ionosphere if they have sufficient energy.

[28] The model for all cases was run to a steady state solution, a point where the time dependent equations produce a solution that did not change with time. In Figures 2 and 3 the top panel shows the density profiles for the summer and winter conditions, respectively, for a K_p value of 5 and for noon local time. The middle panel shows the velocity profiles, and the bottom panel shows the density profiles for the neutral (thermal) and geocoronal (hot) atoms. The main differences between the winter and summer cases are that the height of the protonosphere decreases from the summer case to the winter case, and that the height of the transition to collisionless conditions drops. The drop in the height of the transition to the collisionless conditions is evident in the velocity plots in Figures 2 and 3. Specifically, the collisionless transition is evident in the velocity profiles in that the H^+ ions accelerate to greater speeds and the O stream particles velocity goes from negative, as the atoms fall from higher altitudes, to near zero as they drop through the collisionless transition region.

[29] As stated above, the values of interest in this study are the neutral polar wind parameters. As seen from Figures 2 and 3, the O stream particles tend to be created at any given altitude, and at heights greater than the collisionless transition, the O particles tend to fall due to the pull of gravity. Figure 4 demonstrates this by showing the production and loss rates for summer solar maximum conditions. There is considerably more production of O stream particles than loss at all altitudes, and because the O^+ has a small vertical velocity, the O steam particles are created almost stationary. Since they are mainly acted upon by the gravitational acceleration after their creation, the O particles flow downward. The O stream particles then enter the collision-dominated region and are quickly decelerated to zero velocity. Thus the O stream characteristics tend to show a negative flux at high altitudes and a small flux at low altitudes.

[30] The most interesting feature of the neutral polar wind concerns the H stream. The neutral H stream tends to be controlled by the changing physical conditions, and by varying geomagnetic conditions, as shown in Figure 5. For summer solstice and solar maximum conditions, the tendency is for the neutral H stream particles to increase with increasing magnetic activity, and to have a larger flux at noon, as compared to midnight. For winter solstice and solar minimum, the variance between noon and midnight is not so evident, but the increase of the neutral H flux with increasing magnetic activity is still evident. The previous Figure 4 shows the production and loss for neutral H stream particles, which indicates that the neutral H steam production and loss rates are in near equilibrium at low altitudes, with production dominating at higher altitudes.

[31] It should be noted that the calculated H stream fluxes are high, on the order of a few 10^9 cm^{-2} s^{-1}. This means that a large amount of H^+ must be converted, through charge exchange, into neutral H. In order to check this, the H^+ loss terms were turned off and the model was run to steady state conditions. This resulted in an order of magnitude increase in the H^+ density, as shown in Figure 6. Hence

Table 2. H Stream Boundary Conditions at 500 km for Summer, Solar Maximum, and Winter, Solar Minimum[a]

	H_s n, cm^{-3}	$K_p = 1$ V, km/s	H_s n, cm^{-3}	$K_p = 5$ V, km/s	H_s n, cm^{-3}	$K_p = 8$ V, km/s
Summer	1×10^4(n)	3.0	1×10^4(n)	4.0		
Solar Maximum	5×10^3(m)	4.0	1×10^4(m)	3.0	1.5×10^4(m)	3.0
Winter	5×10^3(n)	4.0	5×10^3(n)	4.0	8×10^3(n)	4.0
Solar Minimum	5×10^3(m)	3.0	5×10^3(m)	4.0	7×10^3(m)	4.0

[a]Here n is for noon, and m is for midnight.

H^+ charge exchange is responsible for the high flux of neutral H.

7. Summary and Discussion

[32] Numerous studies of the polar wind have been conducted since the 1960s, and in just the past 20 years the importance of ENAs has been realized. It has become evident that the neutral streams emanating from the polar regions (the neutral polar wind) are of considerable importance. In order to elucidate their characteristics, numerical simulations were conducted for summer solstice, under solar maximum conditions, and for winter solstice, under solar minimum conditions, thus spanning a range of possible seasonal and solar cycle conditions. The results show that a large escape flux of about 10^9 cm^{-2} s^{-2} can be expected for the neutral H stream under all seasonal conditions considered hear, and for varying solar activity levels. The O stream particles, on the other hand, do not escape in this simulation; they instead tend to flow in the downward direction. This would then limit the O stream escape to some sort of energization process that is not included in this model, such as a geomagnetic storm, precipitating ions, auroral energization, etc.

[33] The one-dimensional simulations in this study are, however, unable to resolve many of the important characteristics of the neutral polar wind. The first is the fact that at low altitudes the plasma $\mathbf{E} \times \mathbf{B}$ drifts across the polar cap with velocities usually in the range of 0.5 to 4 km/s. Since the plasma at low altitudes has a small vertical velocity, the neutral polar wind particles will attain a nearly horizontal velocity equal to the $\mathbf{E} \times \mathbf{B}$ drift velocity. The neutral polar wind particles created at the lower altitudes are a possible source for the geocorona. Additionally, as the ions begin to accelerate along the magnetic field at higher altitudes, the neutral polar wind particles take on a more and more vertical aspect when they are created, thus giving the neutral polar wind a more field-aligned velocity, sending the neutral particles into the magnetosphere if their energies are sufficient. This concept is demonstrated in Figure 7, indicating the height dependence of the neutral polar wind on the height of the charge exchange reaction. Thus, due to the varying directions of the production with height, and the fact that the flux tubes convect around the polar cap, neutral polar wind particles will be created in all directions and with varying velocities.

[34] The scenario shown in Figure 7 might explain the observations of *Wilson et al.* [2003]. The neutral atoms imaged by the LENA instrument on the IMAGE spacecraft are low-energy neutral atoms, and could come from H^+ and O^+, which have been energized in or around the auroral zone. The LENA instrument was designed to image low energy neutral atoms in the range of 10–300 eV. This is well above the energies used in the model. However, during the perigee passes of the IMAGE spacecraft the spacecraft is moving with a sufficient velocity that atoms in the 0.1 to 5 eV range may be seen in the spacecraft frame of reference as having sufficient energies for detection [*Wilson et al.*, 2003]. If the energetic oxygen neutrals could achieve the 0.1–5 eV necessary for detection, through the addition of energization processes to the model, then they would be visible by the LENA instrument. Although a full understanding of the LENA perigee pass signal has not been achieved, it was pointed out that at least part of the signal, concentrated around the ram direction due to the spacecraft motion as explained above, is very likely part of the oxygen

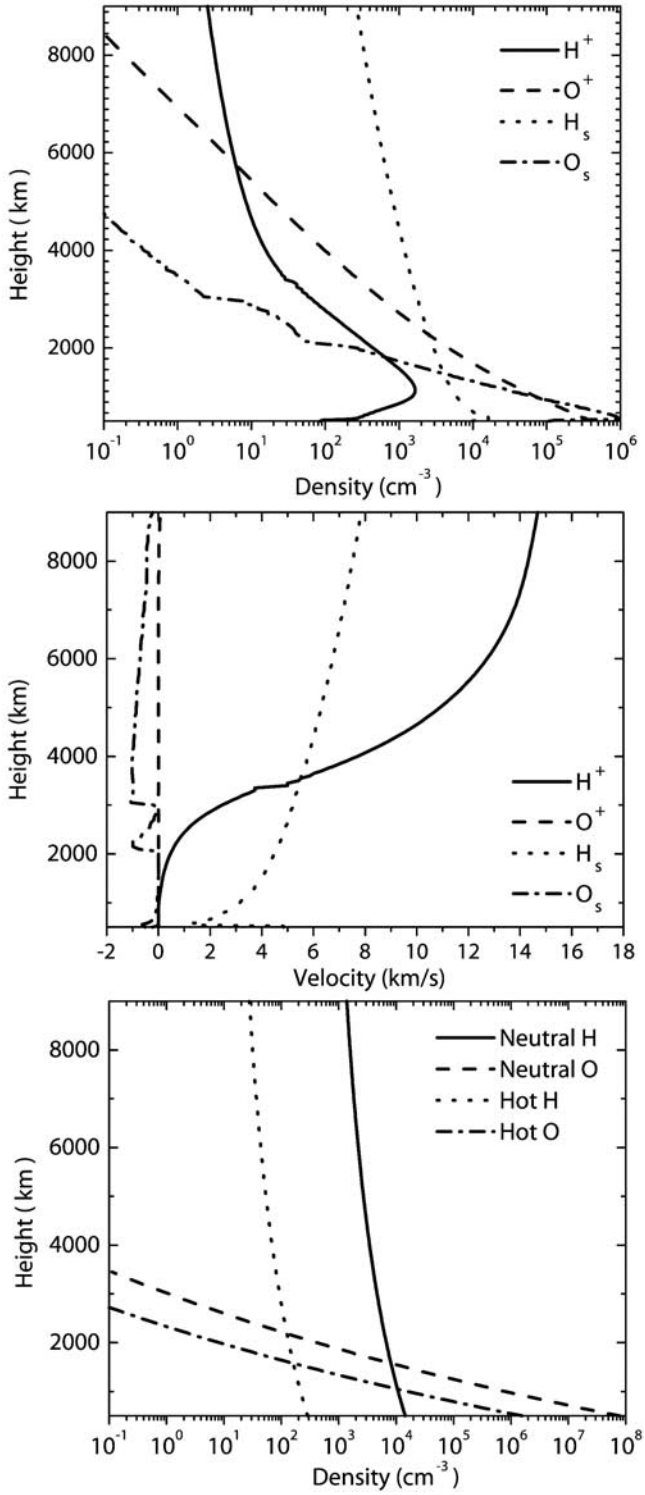

Figure 2. Various plots for summer solstice under solar maximum conditions. The top panel shows the density structure of the polar wind, including the neutral polar wind, the middle panel is the velocity structure, and the bottom panel is the neutral background densities.

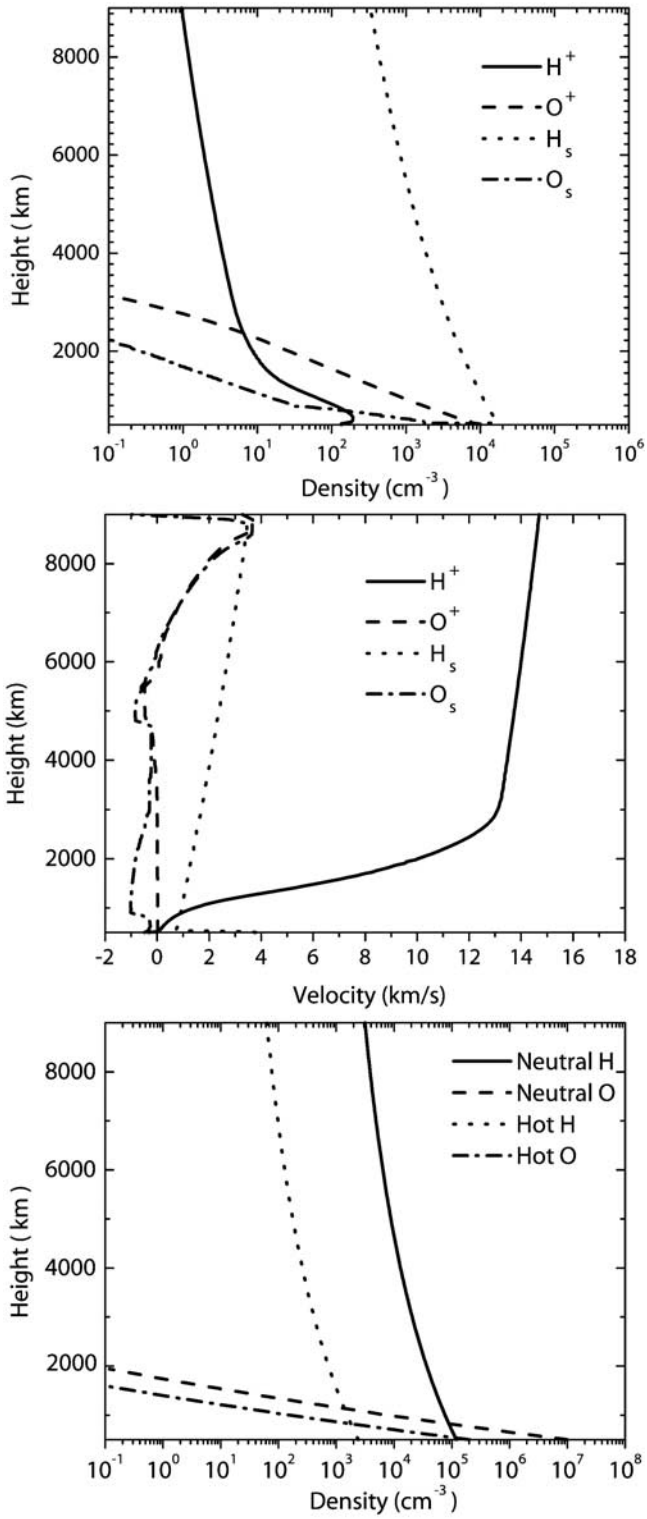

Figure 3. Same as Figure 2, except for winter solstice, solar minimum conditions.

geocorona, and may be produced in many regions, not just the auroral zones. For the part of the signal seen further from the ram direction, more energetic atoms are involved, and these particles may be from auroral zone energization followed by charge exchange with thermospheric oxygen.

[35] However, after a careful analysis of the instrument, *Wilson et al.* [2003] came up with the following main conclusions:

[36] (1) A measurable flux of low-energy (<50 eV) neutral oxygen atoms is always present in the near-Earth environment.

[37] (2) Two main sources of these particles are suggested, one for energies less than 20 eV, and one for energies greater than 20 eV, with the more energetic source also being more variable.

[38] (3) The neutral production rate increases with increasing magnetic activity.

[39] (4) There is a diurnal trend in the data for Southern Hemisphere winter, with the maximum flux values occurring when perigee occurs near 07:40 UT and a minimum flux occurring when perigee occurs near 19:40 UT.

[40] (5) The neutrals imaged near perigee appear to have a broad range of direction so that a localized source, such as the auroral zone, alone cannot produce them.

[41] The mechanism put forth in Figure 7 could possibly explain the low-energy part of the data in the LENA perigee

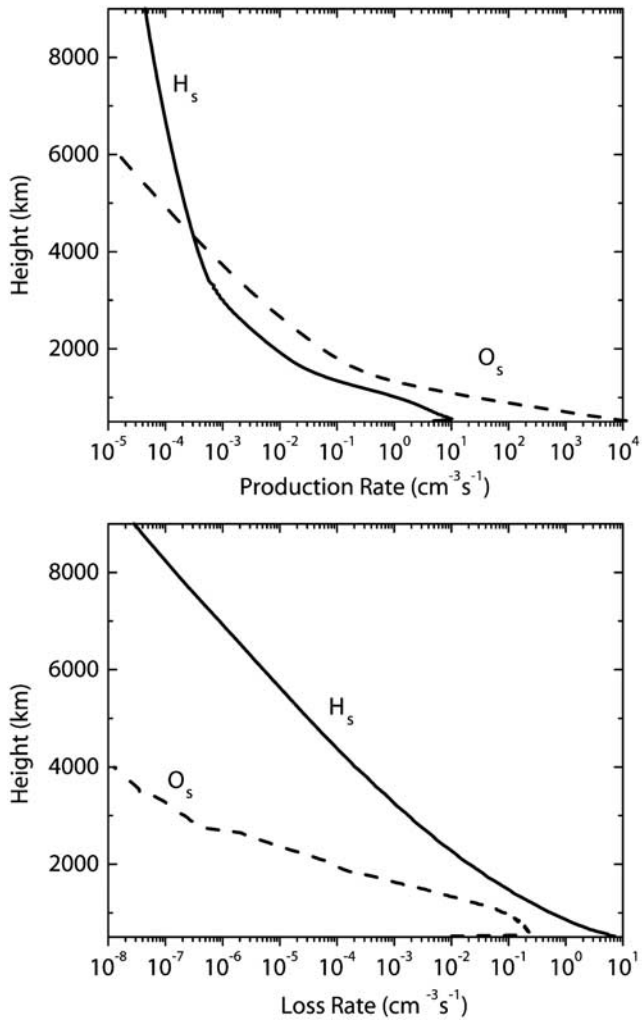

Figure 4. A plot for summer solstice, solar maximum conditions, showing the production (top panel) and loss (bottom panel) rates for the neutral polar wind stream particles.

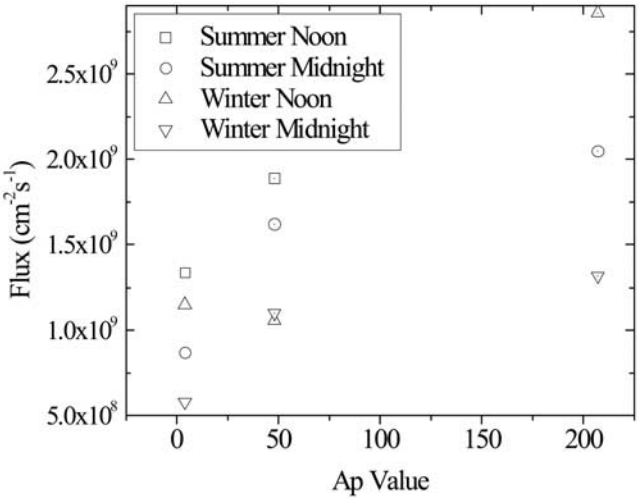

Figure 5. Flux values for the neutral polar wind at 1000 km. The trend in the data is for an increased flux at noon compared to midnight and an increase in flux with increasing magnetic activity.

pass. Figure 7 is an illustration showing a simple two-cell convection pattern, along with several convecting flux tubes. It should be noted that the simple two-cell convection pattern will not be typical, but a more complicated structure will be present, and it will be evolving in time. The flux tubes will convect in a fashion as to follow the electrostatic potential contours, thus providing flux tubes that will be moving in various directions and at varying speeds over much of the polar cap. The flux tubes convecting in different directions, combined with the charge-exchange mechanism, would yield energetic neutrals flowing through a wide angular spread with varying energies. Thus the unexplained broad range of motions observed by *Wilson et al.* [2003] for low-energy energetic neutrals produced at high latitudes might be explained by the neutral polar wind mechanism shown in Figure 7.

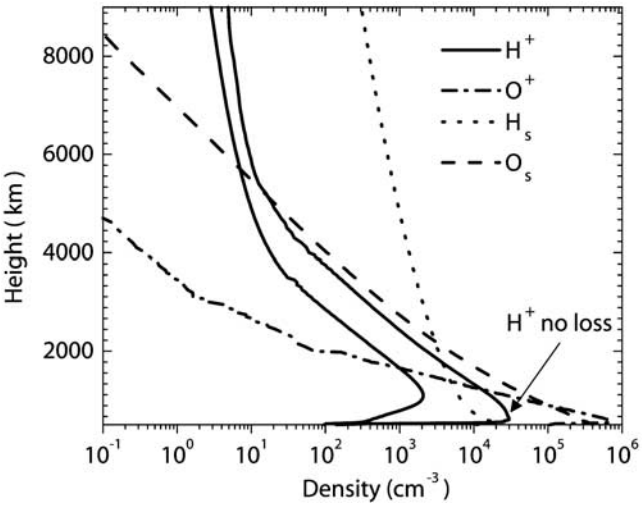

Figure 6. A demonstration of the increase in the amount of H^+ when the loss terms are turned off. Hence there is sufficient H^+ to account for the large flux of H stream particles.

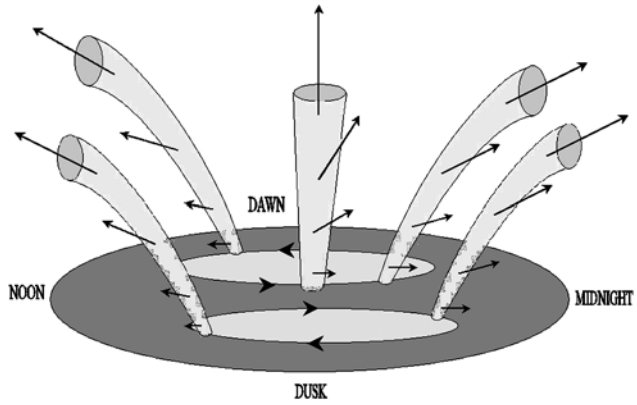

Figure 7. Schematic diagram showing the three-dimensional nature of the neutral polar wind and the production of low-energy neutrals flowing in all directions.

[42] The mechanism shown in Figure 7 should still operate whether or not our neutral polar wind model can explain the LENA data. Specifically, ion outflow along **B** and ion convection across **B** will, after charge exchange, produce energetic neutrals moving in all directions with varying energies at high latitudes. In order for the LENA instrument to image neutrals during a perigee pass in the 0.1–5 eV range, they must be oxygen atoms. This is because a spacecraft velocity of 10 km/s does not provide sufficient energy to hydrogen atoms to put them above the instruments lower detection threshold. Oxygen atoms may be heated to energies of 10–50 eV perpendicular to **B** in the dayside cusp [*Schunk and Nagy*, 2000], or through several other kinetic processes, i.e., wave-particle interactions, hot electrons, or low-altitude energization [*Barakat et al.*, 2003, and references therein], none of which are included in this fluid model to date. All of these additional mechanisms would increase the flux of O that would be visible to the LENA instrument.

[43] **Acknowledgments.** This research was supported by a NASA Graduate Student Research Program Fellowship to L. Gardner via Grant NGT5-142, by the NASA Sun-Earth Connection Theory Program via Grant NAG5-8227, and by NSF Grant ATM-0000171 to Utah State University. We would also like to thank one of the referees for the helpful comments about the LENA instrument.

[44] Arthur Richmond thanks Gordon Wilson and another reviewer for their assistance in evaluating this paper.

References

Axford, W. I. (1968), The polar wind and the terrestrial helium budget, *J. Geophys. Res.*, *73*, 6855–6859.

Axford, W. I. (1969), Magnetospheric convection, *Rev. Geophys.*, *7*, 421–459.

Axford, W. I., and C. O. Hines (1961), A unifying theory of high-latitude geophysical phenomena and geomagnetic storms, *Can. J. Phys.*, *39*, 1433–1464.

Barakat, A. R., and R. W. Schunk (1987), Stability of the polar wind, *J. Geophys. Res.*, *92*, 3409–3415.

Barakat, A. R., R. W. Schunk, and H. G. Demars (2003), Seasonal and solar activity dependence of the generalized polar wind with low-altitude auroral ion energization, *J. Geophys. Res.*, *108*(A11), 1405, doi:10.1029/2002JA009360.

Bisikalo, D. V., V. I. Shematovich, and J. C. Gérard (1995), A kinetic model of the formation of the hot oxygen geocorona: 2. Influence of O^+ ion precipitation, *J. Geophys. Res.*, *100*, 3715–3720.

Boris, J. P., and D. L. Book (1976), Solution of continuity equations by the method of flux-corrected transport, in *Methods in Computational Physics*, vol. 16, edited by B. Alder, S. Fernback, and M. Rotenberg, pp. 85–129, Academic, San Diego, Calif.

Chappell, C. R., T. E. Moore, and J. H. Waite Jr. (1987), The ionosphere as a fully adequate source of plasma for the Earth's magnetosphere, *J. Geophys. Res.*, *92*, 5896–5910.

Cotton, D. M., G. R. Gladstone, and S. Chakrabarti (1993), Sound rocket observation of a hot atomic oxygen geocorona, *J. Geophys. Res.*, *98*, 21,651–21,657.

Demars, H. G., and R. W. Schunk (2002), Three-dimensional velocity structure of the polar wind, *J. Geophys. Res.*, *107*(A9), 1250, doi:10.1029/2001JA000252.

Dessler, A. J., and F. C. Michel (1966), Plasma in the geomagnetic tail, *J. Geophys. Res.*, *71*, 1421–1426.

Eccles, J. V., and W. J. Raitt (1992), Reactive collision terms for fluid transport theory, *Planet. Space Sci.*, *40*, 47–62.

Gérard, J. C., P. G. Richards, V. I. Shematovich, and D. V. Bisikalo (1995), The importance of new chemical sources for the hot oxygen geocorona, *Geophys. Res. Lett.*, *22*, 279–282.

Hays, P. B., and J. C. G. Walker (1966), Doppler profiles of the 5577 Å airglow, *Planet. Space Sci.*, *14*, 1331–1337.

Hedin, A. E. (1989), Hot oxygen geocorona as inferred from neutral exospheric models and mass spectrometer measurements, *J. Geophys. Res.*, *94*, 5523–5529.

Moore, T. E., C. J. Pollick, R. L. Arnoldy, and P. M. Kintner (1986a), Preferential O^+ heating in the topside ionosphere, *Geophys. Res. Lett.*, *13*, 901–904.

Moore, T. E., M. Lockwood, M. O. Chandler, J. H. Waite Jr., C. R. Chappell, A. Persoon, and M. Sugiura (1986b), Upwelling O^+ ion source characteristics, *J. Geophys. Res.*, *91*, 7019–7031.

Nishida, A., N. Iwasaki, and T. Nagata (1966), The origin of fluctuations in the equatorial electrojet: A new type of geomagnetic fluctuation, *Ann. Geophys.*, *22*, 478–484.

Orsini, S., I. A. Daglis, M. Candidi, K. C. Hsieh, S. Livi, and B. Wilken (1994), Model calculation of energetic neutral atoms precipitation at low altitudes, *J. Geophys. Res.*, *99*, 13,489–13,498.

Raitt, W. J., R. W. Schunk, and P. M. Banks (1975), A comparison of the temperature and density structure in high and low speed thermal proton flows, *Planet. Space Sci.*, *23*, 1103–1118.

Richards, P. G., M. P. Hickey, and D. G. Torr (1994), New sources for the hot oxygen geocorona, *Geophys. Res. Lett.*, *21*, 657–660.

Roelof, E. C. (1987), Energetic neutral atom image of a storm-time ring current, *Geophys. Res. Lett.*, *14*(6), 652–655.

Rohrbaugh, R. P., and J. S. Nisbet (1973), Effect of energetic oxygen atoms on neutral density models, *J. Geophys. Res.*, *78*, 6768–6772.

Schunk, R. W., and A. F. Nagy (2000), *Ionospheres*, Cambridge Univ. Press, New York.

Schunk, R. W., and J. J. Sojka (1989), A three-dimensional time-dependent model of the polar wind, *J. Geophys. Res.*, *94*, 8973–8991.

Schunk, R. W., and J. J. Sojka (1997), Global ionosphere-polar wind system during changing magnetic activity, *J. Geophys. Res.*, *102*, 11,625–11,651.

Shelley, E. G., W. K. Perterson, A. G. Ghielmetti, and J. Geiss (1982), The polar ionosphere as a source of energetic magnetospheric plasma, *Geophys. Res. Lett.*, *9*, 941–944.

Shematovich, V. I., D. V. Bisikalo, and J. D. Gérard (1994), A kinetic model of the formation of the hot oxygen geocorona: 1. Quiet geomagnetic conditions, *J. Geophys. Res.*, *99*(A12), 23,217–23,228.

Torr, M. R., and D. G. Torr (1979), Energetic oxygen: A direct coupling mechanism between the magnetosphere and thermosphere, *Geophys. Res. Lett.*, *6*, 700–702.

Torr, M. R., J. C. G. Walker, and D. G. Torr (1974), Escape of fast oxygen from the atmosphere during geomagnetic storms, *J. Geophys. Res.*, *79*, 5267–5271.

Wilson, G. R., T. E. Moore, and M. R. Collier (2003), Low-energy neutral atoms observed near the Earth, *J. Geophys. Res.*, *108*(A4), 1142, doi:10.1029/2002JA009643.

Yee, J. H., and P. B. Hays (1980), The oxygen polar corona, *J. Geophys. Res.*, *85*, 1795–1799.

Yee, J. H., J. W. Meriwether Jr., and P. B. Hays (1980), Detection of a corona of fast oxygen atoms during solar maximum, *J. Geophys. Res.*, *85*, 3396–3400.

L. C. Gardner and R. W. Schunk, Center for Atmospheric and Space Sciences, Utah State University, Logan, UT 84322-4405, USA. (emphyx@yahoo.com)